Mon. Not. R. Astron. Soc. **000**, 1–?? (2002) Printed 16 July 2009 (MN LaTeX style file v2.2)

A Model of Polarized X-ray Emission from Twinkling Synchrotron Supernova Shells

A.M.Bykov[1⋆], Yu.A.Uvarov[1], J.B.G.M.Bloemen[2], J.W. den Herder[2] and J.S.Kaastra[2]
[1] *Ioffe Institute for Physics and Technology, 194021 St.Petersburg, Russia*
[2] *SRON Netherlands Institute for Space Research, Utrecht, The Netherlands*

Accepted 2 July 2009. Received 2009 July 2; in original form 2009 May 2.

ABSTRACT
Synchrotron X-ray emission components were recently detected in many young supernova remnants (SNRs). There is even an emerging class - SN1006, RXJ1713.72-3946, Vela Jr, and others - that is *dominated* by non-thermal emission in X-rays, also probably of synchrotron origin. Such emission results from electrons/positrons accelerated well above TeV energies in the spectral cut-off regime. In the case of diffusive shock acceleration, which is the most promising acceleration mechanism in SNRs, very strong magnetic fluctuations with amplitudes well above the mean magnetic field must be present. Starting from such a fluctuating field, we have simulated images of *polarized* X-ray emission of SNR shells and show that these are highly clumpy with high polarizations up to 50%. Another distinct characteristic of this emission is the strong intermittency, resulting from the fluctuating field amplifications. The details of this "twinkling" polarized X-ray emission of SNRs depend strongly on the magnetic-field fluctuation spectra, providing a potentially sensitive diagnostic tool. We demonstrate that the predicted characteristics can be studied with instruments that are currently being considered. These can give unique information on magnetic-field characteristics and high-energy particle acceleration in SNRs.

Key words: radiation mechanisms: non-thermal—polarization—X-rays: ISM—(ISM:) supernova remnants—shock waves.

1 INTRODUCTION

Electrons and positrons accelerated to TeV energies by diffusive shock acceleration (DSA) in SNR shells will efficiently radiate in X-rays in the associated magnetic fields (e.g., Reynolds & Chevalier 1981). A recent review on 'SNRs at high energy' is given by Reynolds (2008). In some sources (e.g. SN1006, RXJ1713.72-3946 and Vela Jr), the synchrotron component is dominating the X-ray emission, whereas in others such as Cas A it is not easy to distinguish the synchrotron component from the bremsstrahlung emission. Mapping of the *polarized* X-ray emission from SNRs would allow to separate out and study the synchrotron components.

With the high-resolution imaging capability of *Chandra*, likely synchrotron structures are already seen in the X-ray images of various SNRs (e.g., Vink & Laming 2003; Bamba et al. 2006; Patnaude & Fesen 2009). The observed non-thermal emission is concentrated in very thin (arcseconds width) filaments and clumps and has typically a rather steep spectrum with an exponential roll-off. In addition, Uchiyama et al. (2007) reported variability of such X-ray hot spots in the shell of SNR RXJ1713.72-3946 on about a one-year timescale. The thin filamentary structures can be naturally explained in the DSA scenario: options are 1) a narrow spatial extend of the TeV-regime electron population caused by efficient electron cooling due to synchrotron energy losses in the vicinity of the SNR shock with strong magnetic-field amplification (e.g., Vink & Laming 2003; Bamba et al. 2005; Vink 2008) and 2) the observed narrow filaments are limited by magnetic field damping and not by the energy losses of the radiating electrons (e.g., Pohl et al. 2005).

Polarized X-ray emission - *from any source* - was observed so far only in very few cases. Observations of the Crab Nebula with X-ray polarimeters aboard *OSO-8* (Novick et al. 1972; Weisskopf et al. 1976) revealed a polarized flux of about 15% at few keV energies (also detected with the *IBIS* detector on *INTEGRAL* by Forot et al. (2008)). Recently, Götz et al. (2009) reported variable polarized emission at 200-800 keV from GRB 041219A with *IBIS*. Very little else can be reported thus far.

Efficient DSA of protons and electrons in supernova shells requires turbulent magnetic fields, with energy den-

⋆ E-mail:byk@astro.ioffe.ru

sities that are a substantial fraction of the shock ram pressure (e.g., Blandford & Eichler 1987; Malkov & Drury 2001; Hillas 2005; Bell 2004; Amato & Blasi 2006; Vladimirov et al. 2006). Both regular and stochastic magnetic fields determine the spectra and maps of synchrotron radiation of high-energy electrons and positrons from SNRs.

A model of non-thermal *radio* emission from SNRs, accounting for the orientation of the regular ambient magnetic field, was presented recently by Petruk et al. (2009). These authors synthesized radio maps of SNRs, making various assumptions on the dependence of the electron injection efficiency on the shock obliquity. Their method uses the azimuthal profile of the radio surface brightness as a probe of the orientation of the ambient magnetic field. The effect of random magnetic fields in supernova shells on radio synchrotron emission was addressed by Stroman & Pohl (2009). They discussed the emission and transport of polarized radio-band synchrotron radiation near the forward shocks of young shell-type supernova remnants with a strong amplification of the turbulent magnetic field. Modeling the magnetic turbulence was done as a superposition of waves at a particular moment in time; no time evolution was considered. They found that isotropic strong turbulence produces only weakly polarized radio emission even in the absence of internal Faraday rotation. If anisotropy is imposed on the magnetic-field structure, then the degree of polarization can be significantly increased, if the internal Faraday rotation is inefficient.

It has long been known that random directions of magnetic fields in addition to Faraday rotation may strongly reduce the *average* polarization of synchrotron emission sources (e.g., Westfold 1959; Crusius & Schlickeiser 1986; Stroman & Pohl 2009). This explains the relatively low polarization frequently observed for radio synchrotron sources. However, as we will show below, the turbulent magnetic fields that reduce the *average* polarization can result in highly polarized patchy structures potentially observable in high resolution images at X-rays.

Reynolds (1998) simulated X-ray synchrotron images assuming a regular magnetic field and distributions of ultra-relativistic electrons accelerated by a forward shock using age-limited and loss-limited parameterizations.

The effect of turbulent magnetic fluctuations (including field *magnitude* fluctuations) on synchrotron X-ray emission images was recently addressed by Bykov et al. (2008). A system of finite size filled with a random magnetic field was modeled and used to construct synchrotron emission maps of a source with kinetically simulated distributions of ultra-relativistic electrons. The random field was composed of a superposition of magnetic fluctuations (transverse plane waves propagating with some phase velocity) with random phases and a given spectrum of amplitudes. Accounting for the field *magnitude* fluctuations was especially important in view of the dependence of the emissivity on the local magnetic field (further addressed below). A particulary strong dependence occurs in the cut-off regime of the synchrotron spectrum (also further addressed below). Bykov et al. (2008) found that non-steady structures (dots, clumps, and filaments) typically arise, in which the magnetic field reaches exceptionally high values. These magnetic-field concentrations dominate the synchrotron maps, with an evolving, intermittent, and clumpy appearance. The modeling showed that the overall efficiency of synchrotron radiation from the cut-off regime of the electron spectrum can be strongly enhanced in a turbulent field with some $\sqrt{\langle B^2 \rangle}$, compared to emission from a uniform field of the same magnitude $\sqrt{\langle B^2 \rangle}$, but of just a random direction. Strong temporal variations of the brightness of small structures were found, with time scales much shorter than variations in the underlying particle distribution. The variability time scale depends on the phase velocity and the spectrum of magnetic fluctuations. The simulated structures indeed resemble the 'twinkling' structures that are observed in X-ray images of some supernova remnants.

The same electrons that are producing X-ray synchrotron emission will emit TeV photons by inverse-Compton scattering. Both processes are of fundamental importance for our understanding of high-energy particle acceleration and the distinction between leptonic and nucleonic contributions to the observed gamma-ray emission (e.g., Aharonian et al. 2007, 2009). Gamma-ray images of a SNR with efficient DSA in different circumstellar environments were constructed by Lee et al. (2008).

In this paper we expand upon the work of Bykov et al. (2008), modeling the specific features of the polarized synchrotron emission arising from the stochastic nature of magnetic fields of young SNR shells. In §2 we describe the simulation setup that includes the kinetic model of a TeV regime electron distribution and a simulation of a random magnetic field with different fluctuation spectra. In §3 we present the resulting polarized synchrotron emission maps for different X-ray energies and different magnetic fluctuation spectra. In §4 we discuss the observational perspective.

2 THE MODEL

In order to construct maps of polarized synchrotron emission from SNR shells, it is convenient to use the local densities of the Stokes parameters. Because of the additive property of the Stokes parameters $\tilde{I}, \tilde{Q}, \tilde{U}, \tilde{V}$ for incoherent photons, we can integrate these over the line of sight weighted with the distribution function of radiating particles. The degree of polarization is determined in a standard way as $\Pi = \sqrt{Q^2 + U^2 + V^2}/I$.

The synchrotron emission is characterized by a coherence length l_f that is of the order of a MeV electron gyroradius (see e.g. Rybicki & Lightman 1979). In the simulation we only consider the effects of magnetic fluctuations having scales that are much larger than $l_f \sim m_e c^2/e\sqrt{\langle B^2 \rangle}$. This is because in the nonlinear DSA modeling of non-relativistic SNR shocks the magnetic fluctuation spectra are expected to fall down steeply at spatial scales below the gyro-radius of a GeV proton (see for instance Fig.3 in Vladimirov et al. 2006). That means that the fluctuation wavenumbers k satisfy $k \cdot l_f \ll 1$. Therefore, neglecting the magnetic fluctuations of the scale less or comparable to l_f, we apply the standard formulae (see e.g. Ginzburg & Syrovatskii 1965) for the synchrotron power of a single particle of Lorentz factor $\gamma \gg 1$ in the simulated random magnetic field composed of the long-wavelength MHD fluctuations. Then we integrate this power over the line of sight through the system filled with random field fluctuations.

The modeling of the polarized synchrotron emission

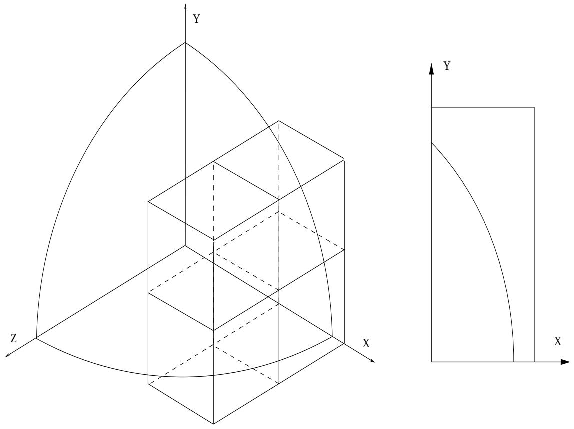

Figure 1. Geometry of the simulated supernova shell. The left panel shows half of the shell quarter with the boxes in which the random magnetic field was simulated. The local densities of the Stokes parameters were then integrated over the line of sight along the axis $-\infty < z < \infty$ (i.e. the two half-quarters of the sphere). The right panel is the resulting projection that is shown in the simulated maps.

from relativistic shocks of GRBs, pulsar wind nebulae and AGNs objects would likely require strong small scale magnetic fluctuations of wavenumbers $k \cdot l_f \sim 1$ and will be discussed elsewhere. The first particle-in-cell simulations of relativistic shocks in unmagnetized electron-positron pair plasmas (see e.g. Spitkovsky 2008) have demonstrated the feasibility of self-consistent modeling of pair acceleration to energies above 100 times that of the thermal energy. The simulated nonthermal particles were carrying about 10% of the downstream thermal energy, promising potential applications to the modeling of polarized synchrotron emission from GRBs, blazars and pulsar wind nebulae.

We start with the spectral flux densities $p_\nu^{(1)}(\theta,\gamma)$ and $p_\nu^{(2)}(\theta,\gamma)$ with two principal directions of polarization radiated by a particle with Lorentz factor γ, as given by Ginzburg & Syrovatskii (1965) [their Eqs.(2.20)]. Here θ is the angle between the local magnetic field $\mathbf{B}(\mathbf{r},t)$ and the direction to the observer. In the case of a random magnetic field it is convenient to use the local spectral densities of the Stokes parameters expressed through $p_\nu^{(1)}$ and $p_\nu^{(2)}$:

$$\hat{\tilde{S}} = \begin{pmatrix} \tilde{I}(\mathbf{r},t,\nu) \\ \tilde{Q}(\mathbf{r},t,\nu) \\ \tilde{U}(\mathbf{r},t,\nu) \\ \tilde{V}(\mathbf{r},t,\nu) \end{pmatrix} = \begin{pmatrix} p_\nu^{(1)} + p_\nu^{(2)} \\ (p_\nu^{(1)} - p_\nu^{(2)}) \cdot \cos 2\chi \\ (p_\nu^{(1)} - p_\nu^{(2)}) \cdot \sin 2\chi \\ (p_\nu^{(1)} - p_\nu^{(2)}) \cdot \tan 2\beta \end{pmatrix}$$

where the angle χ is between the major axis of the polarization ellipse and a coordinate in the plane perpendicular to the observer direction, and $\tan\beta$ is determined by the ratio of the minor and major axes of the ellipse (Ginzburg & Syrovatskii 1965).

2.1 Random magnetic field and particle distribution

Synchrotron X-ray emission is radiated by 10 TeV regime electrons since the magnetic field amplitude in SNR shells is typically below a mG. Efficient DSA of high-energy particles requires a substantial amplification of magnetic field fluctuations in the vicinity of the shock; see e.g. Bell (1978); Blandford & Eichler (1987); Malkov & Drury (2001). Magnetic-field amplification mechanisms due to cosmic-ray instabilities in nonlinear DSA were proposed recently by Bell (2004); Amato & Blasi (2006); Vladimirov et al. (2006); Pelletier et al. (2006); Vladimirov et al. (2008); Zirakashvili & Ptuskin (2008). The models predict amplified magnetic-field amplitudes well above the interstellar field in the far upstream of the shock. These current models are suited to estimate the amplitudes and spectra of amplified magnetic fluctuations averaged over some macroscopic spatial and temporal scales. The averaged magnetic-field spectra available from the models are appropriate to model energetic particle spectra, but do not allow to simulate the synchrotron images of SNR shells and to judge about their temporal evolution.

In reality the distribution of the emitting electrons is a random function of position and particle energy because of the stochastic nature of both the electromagnetic fields and the particle dynamics. However, no self-consistent treatment of such a particle distribution in strong magnetic turbulence is available. Rigorous modeling of the magnetic-field structure and evolution should invoke simultaneously fully nonlinear PIC-type simulations of the collisionless shock, supersonic flow, and the effect of the high-energy particles. A microscopic selfconsistent description of magnetic-field fluctuations that are strongly coupled with electric currents of accelerated particles is not feasible yet for non-relativistic shock simulations in SNRs (see appendix in Vladimirov et al. 2008, for a discussion).

Therefore, to model the synchrotron SNR images we simulated local statistically stationary random magnetic fields of given spectra using the technique described in Bykov et al. (2008). The statistically isotropic and homogeneous random field was constructed as a sum over a large number of plane waves with wave vector, polarization, and phase chosen randomly. In the simulation presented below we assume a plane wave frequency $\omega_n(\mathbf{k}_n) = v_{\rm ph} \cdot k_n$ parameterized with a phase velocity $v_{\rm ph}$. The spectral energy density of the magnetic-field fluctuations of wavenumber k is described as $W(k) \propto k^{-\delta}$, where δ is the spectral index.

$$\langle B^2 \rangle = \int_{k_{\min}}^{k_{\max}} dk\, W(k),$$

The average square magnetic field $\langle B^2 \rangle$, the spectral index δ, and the wavenumber range ($k_{\min}$, $k_{\max}$) are the input parameters of the model. The spectral index δ in the standard DSA scenario is expected to be in the range $1 \leqslant \delta \leqslant 2$.

Then the local spectral emissivity of polarized synchrotron emission was determined at various times using a calculated model distribution of electrons (or positrons). The kinetic model used to simulate the electron distribution was described in detail by Bykov et al. (2000). The spatially inhomogeneous electron distribution function is calculated from the kinetic equation for electrons at a SNR shock that uses piece-wise parametrization of the particle diffusion coefficient to account for both Fermi I and II types accelerations and that is consistent with the magnetic fluctuation spectrum. The model assumes a diffusion coefficient $\kappa(p) \propto p^a$, where $a = 1$ for TeV-regime electrons (the Bohm type diffusion regime) and it has a flatter energy dependence at MeV regime energies. The synchrotron losses of 10 TeV regime electrons in magnetic fields of $\sqrt{< B^2 >} > 10^{-5}$ G are faster than the inverse Compton losses that are dominated by CMB photon scattering.

The scale sizes of the particle distributions of the shock upstream (both electrons and protons) for DSA is $\Delta^u \approx \kappa(p)/u_{\rm sh} \sim 3 \times 10^{17} \cdot u_{\rm sh8} \cdot B_{\mu{\rm G}}^{-1} \cdot E_{TeV}$ cm, where the r.m.s. magnetic field $B_{\mu{\rm G}}$ is in μG units, $u_{\rm sh8}$ is the shock velocity in units of 1,000 km s^{-1}, and E_{TeV} is the electron energy in TeV units. In the shock upstream the width of the layer where the highest energy electrons are stopped due to synchrotron losses is about Δ^u. In the shock downstream the width of the ultra-relativistic electron/positron cooling layer $\Delta_{\rm s}^d$ is about $\Delta^d \sim 6 \times 10^{21} \cdot u_{\rm sh8} \cdot B_{\mu{\rm G}}^{-2} \cdot E_{TeV}^{-1}$ cm. Both widths $\Delta^{u,d}$ of the electron regions emitting X-rays are relatively narrow, typically below 0.3 pc for $B_{\mu{\rm G}} > 30$ and $E_{TeV} \gg 1$. Therefore, for large enough SNR shells of radii $R_{\rm SNR} >> \Delta^{u,d}$ the one dimensional approximation for the determination of the distribution function is well justified. It is also important that the wavelengths of magnetic fluctuations in the SNR shell are of the order of the gyroradii of the relativistic protons in DSA models, and therefore that these are below $\Delta^{u,d}$ justifying the use of a homogeneous r.m.s. field in the losses term of the kinetic equation. We numerically calculated the electron distribution function in the vicinity of the SNR forward shock. The results were then used in simulations of the maps of polarized synchrotron emission of the SNR.

2.2 Geometry

Figure 1 shows a 3-D sketch of the simulated SNR and its projection along the line of sight. To simulate the images of the SNR shell we assumed that a quarter part of a spherical forward shock has a relativistic electron distribution $N(z, \gamma, t)$ that does not depend on the azimuthal and polar angles, but is inhomogeneous in the radial direction with a strong peak (of width $\Delta_{\rm s}$) at the shock position at $r = R_{\rm SNR}$. The line of sight is along the z axis. The Stokes parameters $\tilde{I}, \tilde{Q}, \tilde{U}, \tilde{V}$ for incoherent photons are additive, so we can integrate these over the line of sight weighted with the distribution function of emitting particles $N(z, \gamma, t)$ to get the intensity

$$\hat{S}(\mathbf{R}_\perp, t, \nu) = \int dz\, d\gamma\, N(z, \gamma, t')\ \hat{\tilde{S}}(\mathbf{r}, \gamma, t'). \qquad (1)$$

To collect the photons reaching the observer at the same moment t, we performed an integration over the source depth using the retarded time $t' = t - |\mathbf{r} - \mathbf{R}_\perp|/c$ as argument in $\mathbf{B}(\mathbf{r}, t')$ and $N(\mathbf{r}, E, t')$. The integration grid has a cell size smaller than $L_{\rm min}$. The result is a surface density of Stokes parameters of radiation from the volume along the line of site. The fourth Stokes parameter V is zero in the case of an isotropic electron velocity distribution. In order to achieve a few percent accuracy we integrated over 8000 grid points along the line of sight. The number of pixels in the sky projection is 100×200. The degree of polarization was derived following Ginzburg & Syrovatskii (1965).

Below we present synchrotron images simulated with a steady model distribution of electrons accelerated by a plane shock of velocity 2,000 km s^{-1} propagating in a fully ionized plasma of number density 0.03 cm^{-3}. The kinetic model used to simulate the electron distribution was described in detail by Bykov et al. (2000). The magnetic field in the far-upstream region was fixed at 3 μG and it was assumed that the magnetic-field amplification produces a random field of $\sqrt{\langle B^2 \rangle} = 3 \times 10^{-5}$ G in the shock vicinity. In the random magnetic field simulations we used a wavenumber range $k_{\rm min} < k < k_{\rm max}$, where $L_{\rm min} = 2\pi/k_{\rm max} = 2 \times 10^{-4}\pi \cdot D$ for $\delta = 1.0$ and $L_{\rm min} = 2\pi/k_{\rm max} = 2 \times 10^{-3}\pi \cdot D$ for $\delta = 2.0$, with $L_{\rm max} = 2\pi/k_{\rm min} = 0.2\pi \cdot D$ for both δ values. Here D is the size of a unit cubic box, as shown in Figure 1. The random magnetic field in the simulated SNR shell quarter was divided into 8 such boxes. This number of boxes was chosen to achieve the required accuracy of the integration of the random field along the line of sight. The field in the boxes was simulated as a function of global SNR coordinates as it is shown in Figure 1 (i.e., not just locally in each box). Note that the field was actually simulated in a region larger than the SNR shell and that the box sizes are larger than the sizes of the random filamentary structures that appear.

3 SIMULATED POLARIZATION MAPS OF THE X-RAY SYNCHROTRON EMISSION

Figures 2-4 show examples of the resulting maps at different X-ray energies. The left panels show the synchrotron intensity, the right panels the polarization degree, and the central panels the product of the two. The latter is a measure of the polarized flux and is meant to illustrate that peaks in the polarization-degree map do not necessarily correspond to peak intensities. The images clearly demonstrate 1) the presence of detailed structures - clumps and filaments - produced by the stochastic field topology (for details see Bykov et al. 2008) and 2) that some of these structures emit highly polarized emission (> 30%) at energies of 5 keV and above.

Figure 5 shows the 5 keV map (as in Figure 3), but for a steeper spectrum of magnetic fluctuations ($\delta = 2.0$ rather than 1.0). There is a distinct difference, indicating that for steeper spectra the size of the polarized structures is larger and the degree of polarization of these structures is higher (about 50% for $\delta = 2.0$ and $\sqrt{\langle B^2 \rangle} = 3 \times 10^{-5}$ G).

Irrespective of the precise value of δ, it is clear from Figures 2-5 that the degree of polarization is higher at higher X-ray energies. The physical reason is best illustrated in case of a power-law electron distribution (with spectral index Γ). Namely, the degree of polarization $\tilde{\Pi}$ and the local synchrotron emissivity $\tilde{I}(\mathbf{r}, t, \nu)$ have the following dependencies on Γ: $\tilde{\Pi} \approx (\Gamma+1)/(\Gamma+7/3)$ (i.e. the degree of of polarization $\tilde{\Pi}$ is increasing with Γ) and $\tilde{I}(\mathbf{r}, t, \nu) \propto B^{1/2(\Gamma+1)}$ (i.e. the local emissivity is relatively very high for large B and large Γ) (see e.g., Ginzburg & Syrovatskii 1965; Rybicki & Lightman 1979). In the high-energy cut-off regime the electron spectrum is typically exponential, but the effective index Γ is large indeed and the value increases for electrons emitting at higher frequency ν. This explains the increase of the polarization degree with ν. In addition, the dependency of the emissivity $\tilde{I}$ on B and Γ can lead to a highly polarized bright feature that stands out in the map for even a single strong local field maximum. In lower-energy maps, for which Γ on average is smaller (i.e. well below the cut-off regime), high polarization of a single maximum can be smoothed or washed

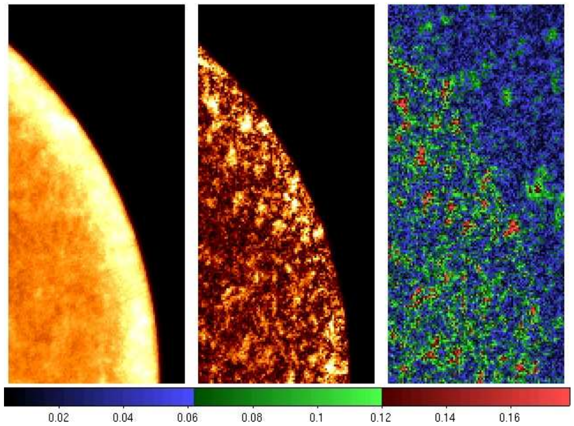

Figure 2. Simulated maps of polarized synchrotron emission in a random magnetic field at 0.5 keV. Intensity, $\nu^2 \cdot I(\mathbf{R}_\perp, t, \nu)$, is shown with a linear color scale in the left panel. The central panel shows the product of intensity and polarization degree. The right panel shows the degree of polarization indicated by the colorbar. The stochastic magnetic field sample has $\sqrt{\langle B^2 \rangle} = 3 \times 10^{-5}$ G and spectral index $\delta = 1.0$.

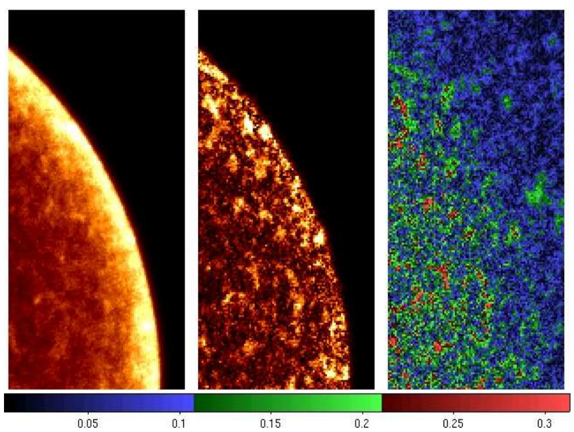

Figure 3. The same maps as in Figure 2, but at 5.0 keV.

out by contributions from a number of weaker field maxima integrated over the line of sight. This effect can be seen in Figures 2-4. The high-energy maps are 'twinkling' because of the finite life-time of the magnetic-field amplifications. The timescale for variations in the polarization (and the energy dependence) is similar to that of the time variability of the intensity maps (studied in §4.1 of Bykov et al. 2008).

Figure 6 illustrates the dependency of the polarization degree on the resolution of the simulated maps ($9''$, $18''$, and $36''$) at 5 keV. In Figures 7 and 8 the polarization maps are presented at 20 keV for larger pixel sizes of $3'$ and $7.5'$ (close to the INTEGRAL ISGRI pixel size) and $\delta = 1$ and 2. Comparison of Figures 7 and 8 shows again the strong dependence on the spectral index δ of the stochastic magnetic field.

4 OBSERVATIONAL PERSPECTIVE

This work was stimulated by the fact that a number of X-ray polarimeter instruments is being considered currently. The

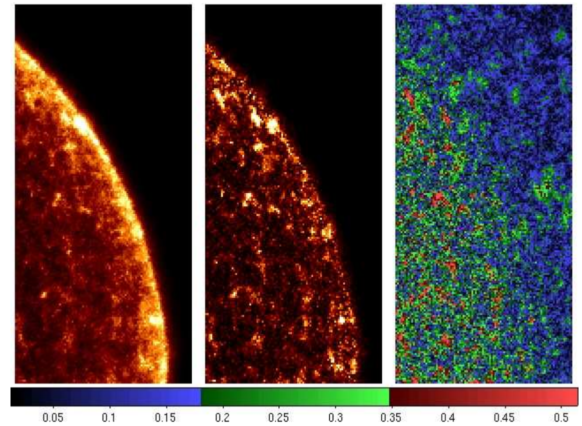

Figure 4. The same maps as in Figure 2, but at 50.0 keV.

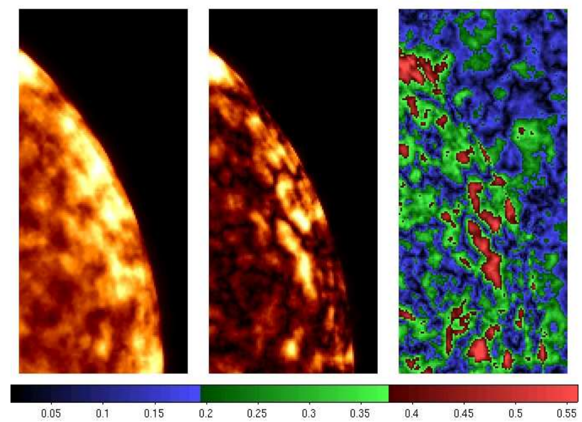

Figure 5. The 5.0 keV synchrotron map for a different magnetic field spectrum in the shell. The stochastic magnetic field sample has $\sqrt{\langle B^2 \rangle} = 3 \times 10^{-5}$ G and $\delta = 2.0$.

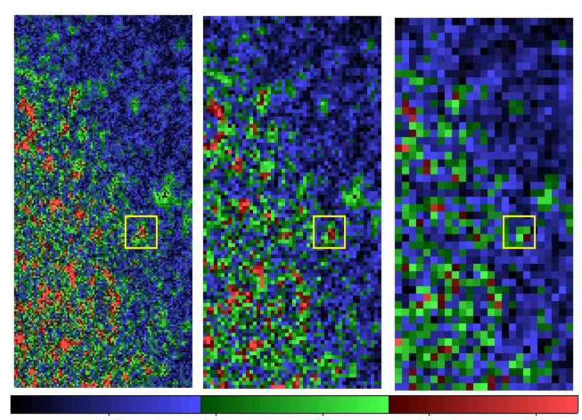

Figure 6. The simulated 5.0 keV synchrotron polarization maps with different pixel sizes. The left one has a pixel size of $9''$, the central of $18''$, and the right of $36''$. The yellow frame of $2.6' \times 2.6'$ indicates the field of view of the *XPOL* polarimeter (see text). The stochastic magnetic field sample has $\sqrt{\langle B^2 \rangle} = 3 \times 10^{-5}$ G and $\delta = 1.0$. The simulated SNR shell has the radius of about 0.4°.

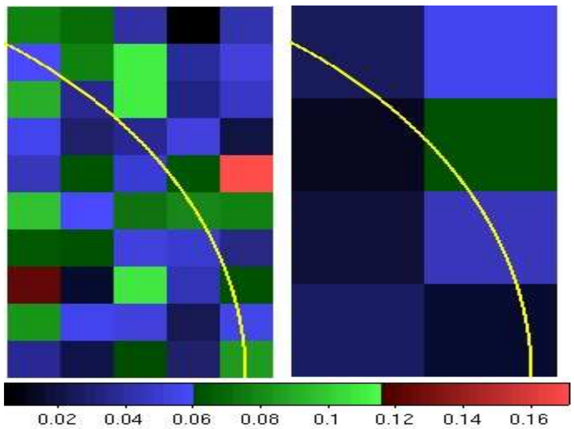

Figure 7. The simulated 20.0 keV synchrotron polarization maps with different pixel sizes. The left one has a pixel size of $3'$ and the right of $7.5'$. The yellow line indicates the forward shock position. The stochastic magnetic field sample has $\sqrt{\langle B^2 \rangle} = 3 \times 10^{-5}$ G and $\delta = 1.0$. The field was simulated in a box larger than the SNR shell, but the regions well outside the forward shock are dim as it is clearly seen in the left panels in Figures 2 - 5.

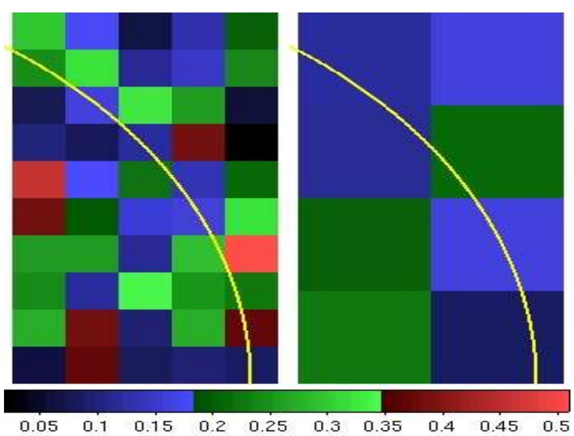

Figure 8. The same maps as in Figure 7, but for magnetic turbulence with $\delta = 2.0$.

Imaging X-ray Polarimetry Explorer *IXPE* was proposed by Weisskopf et al. (2008) as a dedicated X-ray-polarimetry observatory to measure the X-ray linear polarization as a function of energy, time, and position. Legere et al. (2005) is developing a Compton polarimeter to measure polarization of hard X-rays in the 50-300 keV energy range. A balloon-borne hard X-Ray polarimeter *HX-POL* is proposed by Krawczynski et al. (2008). A Hard X-ray Telescope *HET* aboard the Energetic X-ray Imaging Survey Telescope *EXIST* (Grindlay 2009), with a wide field of view for the coded aperture imaging, is being designed to study the polarization at high energies and its temporal evolution. Polarization detection of X-ray sources as faint as 1 milliCrab is an aim of the Gravity and Extreme Magnetism SMEX *(GEMS)* mission that uses foil mirrors and Time Projection Chamber detectors (Swank et al. 2008; Jahoda et al. 2008). The missions listed above have good perspectives in this field of research. We address here the potentials of the *XPOL* polarimeter as proposed for XEUS (Costa et al. 2008) - although evolved into International X-ray Observatory (*IXO*) in the mean time - to illustrate the observational possibilities for synchrotron X-ray studies of SNR RXJ1713.72-3946 as a generic example.

RXJ1713.72-3946 has an extended shell of about one degree angular diameter. A field of view of $1.5' \times 1.5'$ and an angular resolution of $5''$ was proposed by Costa et al. (2008), if *XPOL* was part of the *XEUS* mission. A polarimeter like *XPOL* aboard the *IXO* mission [1] will have a somewhat larger field of view. We illustrate that case in Figure 6 where the field of view of $2.6' \times 2.6'$ is shown as a yellow box in the polarization maps simulated with pixel sizes of $9''$, of $18''$, and of $36''$ to illustrate the angular resolution effect.

In the case of an extended source like RXJ1713.72-3946 first of all a wide field map of the source region is needed to specify the *XPOL* pointing. Using *Chandra* archive data, we estimate the 2-10 keV flux from a $2.6' \times 2.6'$ region in the shell of RXJ1713.72-3946 to be about 4.5×10^{-12} erg cm^{-2} s^{-1}. From the minimum detectable polarization as a function of observing time as presented in Fig. 6 of Costa et al. (2008), corrected for the reduced effective area of *IXO*[1], we estimated that a meaningful polarization map can be constructed with *XPOL* within an exposure time of 100 ks. The polarization map of $2.6' \times 2.6'$ should likely reveal detailed highly-polarized structures with typical scales of about $10''$ as it was discovered in *Chandra* images by Uchiyama et al. (2007). The degree of polarization will increase with increasing X-ray energy as predicted from the modeling in this paper. The polarization will be time variable on a few year time scale (depending on the photon energy) as it was found by Bykov et al. (2008) in simulated intensity maps. Mapping of the whole extended shell of RXJ1713.72-3946 in polarized X-rays would be unrealistic with that set up, therefore the target must be first identified with a wide field X-ray imager.

Another object of great interest is Cas A, that is of an angular size comparable with the field of view of *XPOL*. We estimate that some thin peripheral polarized X-ray filaments of some ten arcsecond scale can be studied with *XPOL*, also with an exposure of about 100 ks. In the DSA model the scale size $L_{\max}$ of the magnetic fluctuations responsible for the twinkling polarized structures is expected to be connected to gyroradii of accelerated protons at maximal energies. These can be roughly estimated to be about $3 \times 10^{17} \cdot B_{\mu\mathrm{G}}^{-1} \cdot E_{100TeV}$ cm. Therefore, their angular sizes are expected to be above a few arcseconds for SNRs within a few kiloparsec distance.

5 CONCLUSIONS

We have studied the *polarization* of X-ray synchrotron emission from SNRs addressing the significant effect of magnetic-field fluctuations on synchrotron emission in X-rays. Such magnetic fluctuations form a natural starting point because they must be present if diffusive shock acceleration is indeed the basic mechanism for accelerating particles in SNRs. Like Bykov et al. (2008) we simulated random magnetics field to construct synchrotron emission maps, given a smooth and

[1] http://ixo.gsfc.nasa.gov/science/performanceRequirements.html

steady distribution of electrons, but now with special attention to the polarization of the resulting emission. The simulated random magnetic fields show *non-steady localized structures with exceptionally high magnetic-field amplitudes*. These magnetic-field concentrations dominate the synchrotron emission - integrated along the line of sight - from energetic >TeV electrons, i.e. in the cut-off regime. In terms of a power-law electron spectrum with spectral index Γ, this can be understood since the synchrotron emissivity $\tilde{I}(\mathbf{r}, t, \nu)$ is proportional to $B^{1/2(\Gamma+1)}$ (i.e. the local emissivity is relatively very high for large B and large Γ). The power-law approximation is only useful over a narrow electron energy range in the cut-off regime, where the effective spectral index Γ is increasing with the electron energy.

Starting from the simulated magnetic-field simulations, we have constructed maps of *polarized* X-ray emission of SNR shells. These are highly clumpy with high polarizations up to 50%. This characteristic of high polarization again applies to energetic >TeV electrons in the cut-off regime. In terms again of a power-law electron spectrum with spectral index Γ, this can be understood since the degree of polarization is given by $\tilde{\Pi} \approx (\Gamma+1)/(\Gamma+7/3)$ (i.e. $\tilde{\Pi}$ is increasing with Γ).

The distinct characteristic of the modeled synchrotron emission is its strong intermittency, directly resulting from the exceptionally high magnetic-field amplifications randomly occurring as shown in the simulations. Also characteristic is the increase of the polarization degree with X-ray energy addressed in §3. Since this "twinkling" polarized X-ray emission of SNRs depends strongly on the magnetic-field fluctuation spectra, it provides a potentially sensitive diagnostic tool.

The intermittent appearance of the polarized X-ray emission maps of young SNR shells can be studied in detail observationally with imagers of a few arcsecond resolution, though even arcmin resolution images can provide important information as it is illustrated in Figures 6,7,8. The polarized emission clumps of arcsecond scales are time variable on a year or longer (depending on the observed photon energy, magnetic field amplification factor and the plasma density in the shell) allowing for rather long exposures even in the hard X-ray energy band. Hard X-ray observations in the spectral cut-off regime are the most informative to study the magnetic fluctuation spectra and the acceleration mechanisms of ultra-relativistic particles.

Altogether, the modeled appearance and its time variability - on a timescale of typically a year - resembles closely what is observed already in X-ray images of some young supernova remnants. Observing the predicted high polarization in clumps and filaments, however, should probably await future instruments that are currently being considered. Such observations will provide unique information on magnetic fields and high-energy particle acceleration in SNRs.

ACKNOWLEDGMENTS

We thank the anonymous referee for careful reading of our paper and a useful comment. Some of the calculations were performed at the Supercomputing Centre (SCC) of the A.F.Ioffe Institute, St.Petersburg. A.M.B. thanks R.Petre for a discussion of the *SMEX* project perspective. A.M.B. and Yu.A.U were supported in part by RBRF grant 09-02-12080 and by the RAS Presidium Programm. SRON is supported financially by NWO, the Netherlands Organisation for Scientific Research.

REFERENCES

Aharonian F., Akhperjanian A. G., Bazer-Bachi A. R., et al. 2007, A&A, 464, 235
Aharonian F., Akhperjanian A. G., de Almeida U. B., et al. 2009, ApJ, 692, 1500
Amato E., Blasi P., 2006, MNRAS, 371, 1251
Bamba A., Yamazaki R., Yoshida T., et al. 2005, ApJ, 621, 793
Bamba A., Yamazaki R., Yoshida T., et al. 2006, Advances in Space Research, 37, 1439
Bell A. R., 1978, MNRAS, 182, 147
Bell A. R., 2004, MNRAS, 353, 550
Blandford R., Eichler D., 1987, Phys. Rep., 154, 1
Bykov A. M., Chevalier R. A., Ellison D. C., et al. 2000, ApJ, 538, 203
Bykov A. M., Uvarov Y. A., Ellison D. C., 2008, ApJ, 689, L133
Costa E., Bellazzini R., Bregeon J., et al. 2008, in Proc. of SPIE Vol. 7011. pp 70110F–1
Crusius A., Schlickeiser R., 1986, A&A, 164, L16
Forot M., Laurent P., Grenier I. A., et al. 2008, ApJ, 688, L29
Ginzburg V. L., Syrovatskii S. I., 1965, ARA&A, 3, 297
Götz D., Laurent P., Lebrun F., et al. 2009, ApJ, 695, L208
Grindlay J. E., 2009, in Bulletin of the American Astronomical Society Vol. 41. p. 388
Hillas A. M., 2005, Journal of Physics G Nuclear Physics, 31, 95
Jahoda K., Black K., Deines-Jones P., et al. 2008, in AAS/High Energy Astrophysics Division p. 28.15
Krawczynski H., Garson III A., Li Q., et al. 2008, ArXiv e-print 0812.1809
Lee S.-H., Kamae T., Ellison D. C., 2008, ApJ, 686, 325
Legere J., Bloser P. L., Macri J. R., et al. 2005, in Proc. of SPIE Vol. 5898. p. 413
Malkov M. A., Drury L., 2001, Reports on Progress in Physics, 64, 429
Novick R., Weisskopf M. C., Berthelsdorf R., et al. 1972, ApJ, 174, L1
Patnaude D. J., Fesen R. A., 2009, ApJ, 697, 535
Pelletier G., Lemoine M., Marcowith A., 2006, A&A, 453, 181
Petruk O., Dubner G., Castelletti G., et al. 2009, MNRAS, 393, 1034
Pohl M., Yan H., Lazarian A., 2005, ApJ, 626, L101
Reynolds S. P., 1998, ApJ, 493, 375
Reynolds S. P., 2008, ARA&A, 46, 89
Reynolds S. P., Chevalier R. A., 1981, ApJ, 245, 912
Rybicki G. B., Lightman A. P., 1979, Radiative processes in astrophysics, Wiley-Interscience, New York
Spitkovsky A., 2008, ApJ, 682, L5
Stroman W., Pohl M., 2009, ApJ, 696, 1864
Swank J., Kallman T., Jahoda K., 2008, in 37th COSPAR Scientific Assembly Vol. 37. p. 3102

Uchiyama Y., Aharonian F. A., Tanaka T., et al. 2007, Nat, 449, 576

Vink J., 2008, in Aharonian F. A. e. a., ed., AIP Conf. Ser. Vol. 1085, Multiwavelength Signatures of Cosmic Ray Acceleration by Young Supernova Remnants. p. 169

Vink J., Laming J. M., 2003, ApJ, 584, 758

Vladimirov A., Ellison D. C., Bykov A., 2006, ApJ, 652, 1246

Vladimirov A. E., Bykov A. M., Ellison D. C., 2008, ApJ, 688, 1084

Weisskopf M. C., Bellazzini R., Costa E., et al. 2008, in Proc. of SPIE Vol. 7011. pp 70111I–1

Weisskopf M. C., Cohen G. G., Kestenbaum H. L., et al. 1976, ApJ, 208, L125

Westfold K. C., 1959, ApJ, 130, 241

Zirakashvili V. N., Ptuskin V. S., 2008, ApJ, 678, 939